DOI: 10.1002/ejic.200800367

MCM-41 Derivatised with Pyridyl Groups and Its Use as a Support for Luminescent Europium(III) Complexes

Sofia M. Bruno,[a] Ana C. Coelho,[a] Rute A. S. Ferreira,[b] Luís D. Carlos,[b] Martyn Pillinger,[a] Anabela A. Valente,[a] Paulo Ribeiro-Claro,[a] and Isabel S. Gonçalves*[a]

Keywords: Mesoporous materials / Lanthanides / Luminescence / Pyridine / β-Diketone

An organic–inorganic hybrid ligand silica was prepared by reaction of the ordered mesoporous silica MCM-41 with 3-triethoxysilylpropyl 4-pyridylacetamide. Elemental analysis indicated that a pyridyl group loading of 0.93 mmol g^{-1} was achieved. The derivatised material was further characterised by powder X-ray diffraction, N_2 adsorption, thermogravimetric analysis, FTIR and Raman spectroscopy, and ^{13}C and ^{29}Si CP MAS NMR spectroscopy. Pyridyl-functionalised MCM-41 (L′′) was treated with chloroform solutions of lanthanide tris-β-diketonate complexes $Ln(nta)_3(H_2O)_2$ [Ln = Eu, Gd; nta = 1-(2-naphthoyl)-3,3,3-trifluoroacetonate] to give the surface-bound monosubstituted species $Ln(nta)_3(H_2O)(L'')$. The residual coordinated water molecules were subsequently replaced by pyridine (py) or methyl phenyl sulfoxide (mpso) to give immobilised $Ln(nta)_3(py)(L'')$ and $Ln(nta)_3(mpso)(L'')$ species. Photoluminescence studies were carried out at room temperature and 14 K. The emission spectra of the Eu-modified materials were dominated by the typical Eu^{3+} red lines ascribed to transitions between the $^5D_0$ excited state and the ground multiplet ($^7F_{0–4}$), and only very weak or negligible emission from the organic ligands are observed. Variation of the excitation wavelength confirmed that all of the Eu^{3+} ions occupied the same average local environment within each sample. By comparison with the photoluminescence data for the nonsupported $Eu(nta)_3(py)_2$ and $Eu(nta)_3(mpso)_2$ complexes, it is shown that the interaction between the host and guest has a strong effect on the excited states of the organic ligands; Eu^{3+} sensitisation occurs exclusively through the ligands rather than by direct intra-$4f^6$ excitation.

Introduction

The interest in mesoporous materials has undergone rapid growth since the beginning of the 1990s when a family of micelle-templated silicas, known as M41S, was reported.[1] The favourable textural properties of these materials (high surface area and pore volume coupled with narrow pore size distributions) make them very attractive for advanced applications in adsorption, catalysis, environmental clean-up and nanotechnology.[2] In the case of MCM-41, one member of the M41S family, the 1D channels are arranged hexagonally. Reactive functional groups (silanols) on the internal surface allow selective modification with postsynthesis treatments commonly used for amorphous oxide supports.[3]

A large number of mesostructured heterogeneous catalysts and photofunctional materials have been prepared by either grafting or tethering of metal-containing species onto the internal surface of ordered mesoporous materials. In the first method, often referred to as surface organometallic chemistry, the organometallic or metallo-organic precursor molecules react with the nucleophilic silanol groups present on the channel walls to form Si–O–M linkages. Examples include reactions with metallocene derivatives,[4] oxomolybdenum complexes[5] and lanthanide tris-β-diketonates [$Ln(diket)_3$].[6] Subsequent postgrafting treatments are sometimes required to generate the desired surface species. Lanthanide complexes have also been immobilised by using the tethering approach, which involves complexation with ligands covalently anchored to the support.[7] Specifically, $Ln(diket)_3$ complexes (Ln = Eu, Gd, Er, Nd, Yb) were immobilised in mesostructured materials by a ligand-exchange reaction between $Ln(diket)_3(H_2O)_2$ precursors and tethered pyrazolylpyridine[7a] or phen[7b–7d] groups. The interest in the immobilisation of these complexes in mesoporous silicas stems from the fact that the photostability under UV radiation is enhanced and the ligand-to-metal energy transfer could be substantially improved, which therefore increases the emission quantum yield. Furthermore, the nature of the interaction between the surface of the host and the lanthanide-coordinated ligands (covalently anchored or weakly bonded) plays an important role in that energy transfer process.[8]

The photoluminescence properties of lanthanide β-diketonate complexes depend to a large extent on the substitu-

[a] Department of Chemistry, CICECO, University of Aveiro, 3810-193 Aveiro, Portugal
E-mail: igoncalves@ua.pt
[b] Department of Physics, CICECO, University of Aveiro, 3810-193 Aveiro, Portugal

Supporting information for this article is available on the WWW under http://www.eurjic.org or from the author.

ents on the β-diketone ligand; a combination of aromatic and fluoro groups give the best results.[9] The presence of C–F bonds, as opposed to C–H bonds, a higher-energy frequency oscillator, helps reduce nonradiative quenching of lanthanide luminescence. For the same reasons, it is preferable to avoid having water molecules in the first coordination sphere of Ln^{3+}. Apart from monodentate ligands such as dmso, bidentate N ligands such as 2,2′-bipyridine, 1,10-phenanthroline, diazabutadienes and pyrazolylpyridines have been extensively investigated as adducting molecules.[10] By contrast, only a few examples of complexes of the type $Ln(diket)_3(L')(L'')$ with two different ligands can be found in the literature.[11] In the present work, the mesoporous silica MCM-41 has been derivatised with pyridyl groups and treated with the complex $Ln(nta)_3(H_2O)_2$ [Ln = Eu, Gd; nta = 1-(2-naphthoyl)-3,3,3-trifluoroacetonate] to give the surface-bound monosubstituted species $Ln(nta)_3(H_2O)(L'')$. The residual coordinated water molecules can readily be replaced by pyridine (py) or methyl phenyl sulfoxide (mpso), which leads to the species $Ln(nta)_3(py)(L'')$ and $Ln(nta)_3(mpso)(L'')$. The supported materials were characterised by powder X-ray diffraction, N_2 adsorption, thermogravimetric analysis, FTIR and Raman spectroscopy, and photoluminescence spectroscopy. For comparison, the tris-β-diketonate complexes $Eu(nta)_3(py)_2$ and $Eu(nta)_3(mpso)_2$ have also been prepared and characterised.

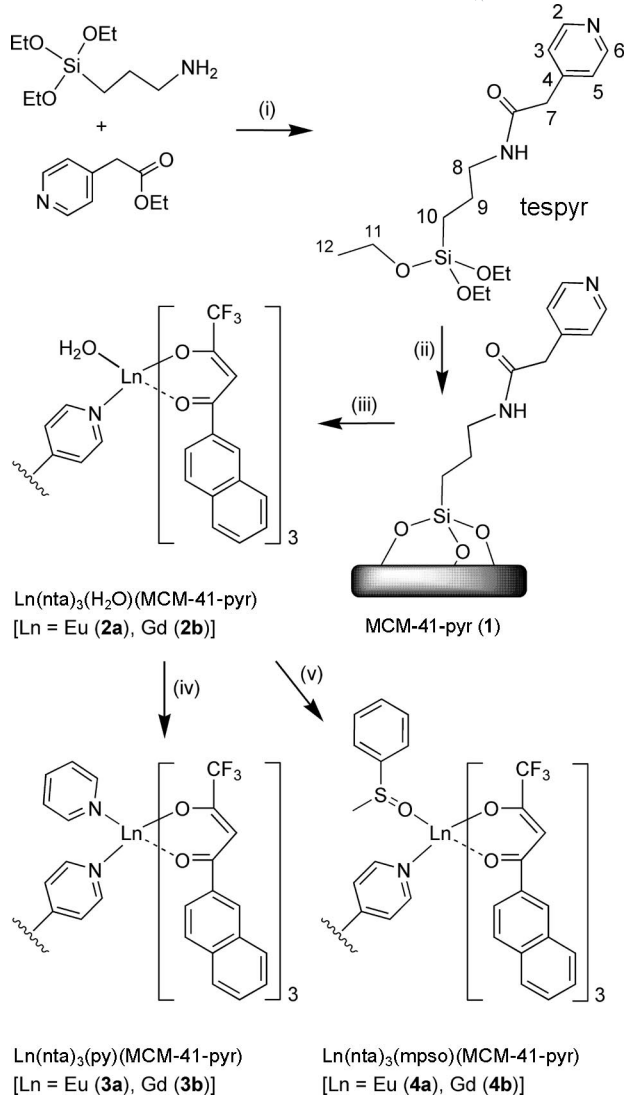

Scheme 1. (i) 48 h, 393 K. (ii) MCM-41, 24 h, toluene, reflux. (iii) $Ln(nta)_3(H_2O)_2$, $CHCl_3$, room temperature. (iv) Pyridine, $CHCl_3$, room temperature. (v) mpso, $CHCl_3$, room temperature.

Results and Discussion

Synthesis

The ligand 3-triethoxysilylpropyl 4-pyridylacetamide (tespyr) was prepared by heating ethyl 4-pyridylacetate (epa) with 1 equiv. 3-triethoxysilylpropylamine (tespa) (Scheme 1). The presence of the amide group in tespyr was confirmed by (i) the IR spectrum, which shows the loss of the carbonyl stretching absorption at 1735 cm^{-1} characteristic of the ester group in epa and the appearance of new bands at 3291 (ν_{NH}) and 1650 cm^{-1} (NHCO); (ii) the ^1H NMR spectrum, which contains a broad resonance at δ = 6.59 ppm for the NH protons; and (iii) the ^{13}C NMR spectrum, which presents a resonance at δ = 168.9 ppm for the NHCO carbon atoms. The purity of the product was confirmed by the absence of signals characteristic of epa or tespa in the NMR spectra.

Treatment of calcined and dehydrated MCM-41 with a solution of tespyr in toluene at reflux gave the modified material MCM-41-pyr (**1**) with a ligand loading of 0.93 mmol g^{-1}, calculated on the basis of the nitrogen content of 2.61 % (Scheme 1). A C/N atomic ratio of 4.7 suggests that most of the ligands were anchored to the silica surface through three Si–O–Si bonds. The efficiency of the grafting process is confirmed by the ^{13}C and ^{29}Si CP MAS NMR spectroscopy (Figure 1 and Figure 2). Unmodified MCM-41 displays two broad overlapping resonances in the ^{29}Si CP MAS NMR spectrum at –100.8 and –107.3 ppm, which correspond to Q^3 and Q^4 species of the silica framework [Q^n = $Si(OSi)_n(OH)_{4-n}$] (Figure 1). A weak shoulder is also observed at δ = –92 ppm for the Q^2 species. The Q^3 sites are associated with single Si–OH groups that include both free and hydrogen-bonded silanols, and the Q^2 sites correspond to geminal silandiols. For the modified material MCM-41-pyr (**1**), two additional signals appear at –57.9 and –64.5 ppm, which can be assigned to T^2 and T^3 organosilica species [T^m = $RSi(OSi)_m(OEt)_{3-m}$], respectively, with T^3 as the major system. In parallel, the relative intensities of the Q^2 and Q^3 resonances decrease with an increase in the intensity of Q^4. The ^{13}C CP MAS NMR spectrum of **1** exhibits lines at 9.1, 22.0 and 41.7 ppm for the three ^{13}C nuclei of the grafted propyl chains and a very weak line at δ = 58.4 ppm attributed to C^{11} of unreacted ethoxysilane groups (Figure 2). The three resonances at 124.7, 147.8 and 171.0 ppm are assigned to the pyridyl ring carbon atoms and the carbonyl group.

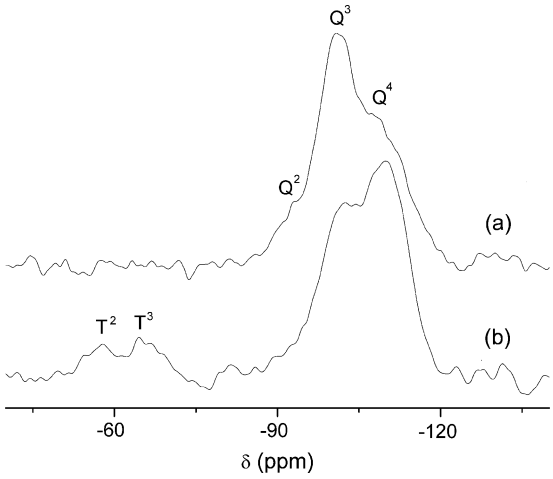

Figure 1. ^{29}Si CP MAS NMR spectra of (a) MCM-41 and (b) MCM-41-pyr (**1**).

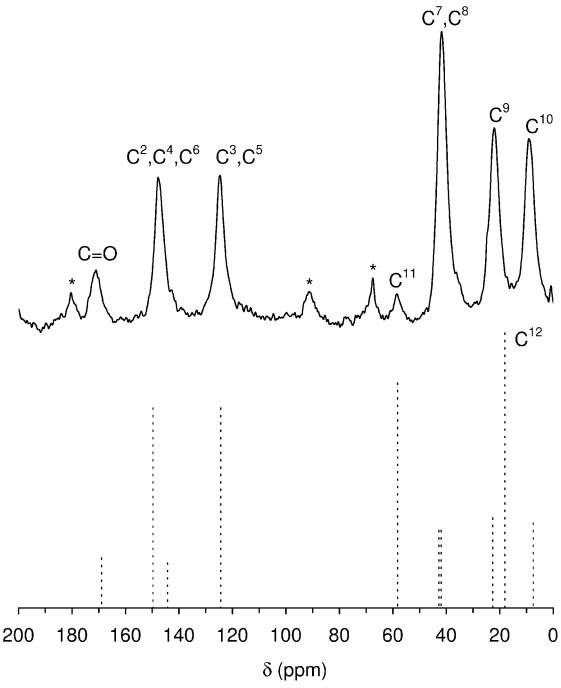

Figure 2. ^{13}C CP MAS NMR spectrum of the modified mesoporous material MCM-41-pyr (**1**) relative to the resonances of the free ligand tespyr (dashed lines give relative intensities). Spinning sidebands are indicated with asterisks.

Figure 3 shows the powder XRD patterns of the MCM-41 starting material and the modified material **1**. The pattern for MCM-41 is characteristic of a well-ordered mesoporous phase and can be indexed as hexagonal with a lattice parameter of 38.50 Å (=$2d_{100}/\sqrt{3}$). The Bragg peaks indexed as (100), (110) and (200) are still observed after the derivatisation step, which indicates retention of the long-range hexagonal symmetry. Compared with MCM-41, the three reflections are shifted to slightly lower 2θ values, which points to an expansion of the unit cell (a = 40.63 Å). Thermogravimetric analysis of **1** shows that the material is thermally stable up to about 473 K (not shown here). The anchored organic moieties decompose in one step between 473 and 823 K with a weight loss of 17.7%, which is intermediate between the calculated values (based on the ligand loading) of 16.5%, with the assumption of complete elimination of ethoxy groups during the grafting step, and 20.6% for retention of one ethoxy group per organosilane group.

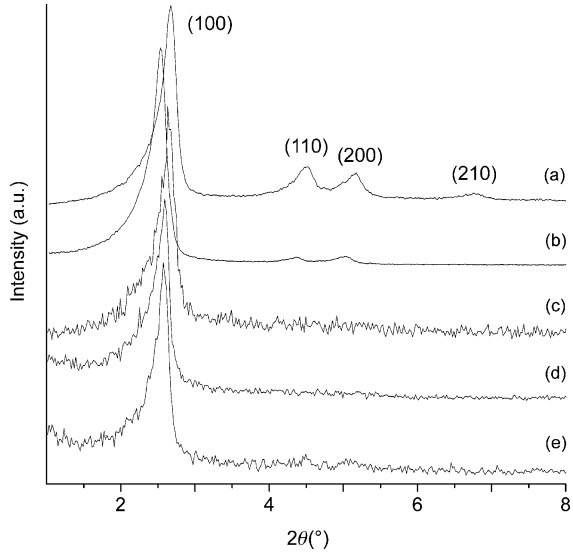

Figure 3. Powder XRD patterns of (a) MCM-41, (b) MCM-41-pyr (**1**), (c) Eu(nta)$_3$(H$_2$O)(MCM-41-pyr) (**2a**), (d) Eu(nta)$_3$(py)(MCM-41-pyr) (**3a**) and (e) Eu(nta)$_3$(mpso)(MCM-41-pyr) (**4a**).

Treatment of **1** with approximately 1 equiv. (with respect to the anchored pyr in **1**) Ln(nta)$_3$(H$_2$O)$_2$ in chloroform gave two supported materials with lanthanide loadings of about 0.8 wt.-% (0.05 mmol g^{-1}), which can be denoted as Ln(nta)$_3$(H$_2$O)(MCM-41-pyr) [Ln = Eu (**2a**), Gd (**2b**)] (Scheme 1). Because of the low lanthanide loadings, which correspond to about 6% of the total pyr loading, the carbon content increased only slightly after the immobilisation steps. Residual coordinated water molecules were subsequently replaced by pyridine or mpso molecules to give the materials designated as Ln(nta)$_3$(py)(MCM-41-pyr) [Ln = Eu (**3a**), Gd (**3b**)] and Ln(nta)$_3$(mpso)(MCM-41-pyr) [Ln = Eu (**4a**), Gd (**4b**)]. The lower lanthanide content for materials **3a** and **3b** (ca. 0.034 mmol g^{-1}) show that partial leaching of the tris-β-diketonate complexes occurred during the reactions. The large excess of pyridine used probably resulted in replacement of both coordinated water and pyr ligands in some of the anchored complexes by pyridine molecules to give the soluble species Ln(nta)$_3$(py)$_2$. This likelihood was verified by preparing the complex Eu(nta)$_3$(py)$_2$ (**5**) by treatment of Eu(nta)$_3$(H$_2$O)$_2$ with pyridine in chloroform (see the Experimental Section for full details and characterisation data). Complex **5** is soluble in chlorinated solvents, diethyl ether, toluene, THF, acetonitrile and ethanol, and insoluble in hexane. For the modified materials **4a** and **4b**, the final lanthanide content of about 0.047 mmol g^{-1} indicates that lanthanide ion leaching was

less significant during the treatment of **2a** and **2b** with mpso. In Scheme 1, it is assumed that mpso coordinates to the metal ions by the sulfoxide oxygen atom rather than the sulfur atom. This type of coordination mode seems the most likely based on previous structural studies of dmso solvates of lanthanide(III) ions[12] and on a comparison with the model complex $Eu(nta)_3(mpso)_2$ (**6**), which was prepared by treatment of $Eu(nta)_3(H_2O)_2$ with mpso in chloroform. In the FTIR spectrum of **6**, bands in the 1000–1100 cm^{-1} range are assigned to phenyl and S–O vibrations. A new band at 1017 cm^{-1} can be tentatively assigned as the S–O stretching vibration. By analogy with the known behaviour for dmso, the downshift of this band relative to that for liquid mpso (1070 cm^{-1}) is consistent with the presence of O-bonded mpso ligands.[12]

Powder XRD measurements of **2a**, **3a** and **4a** show that the expansion of the unit cell detected for the ligand-silica **1** is less pronounced, since the (100) reflection for all three materials is almost unshifted relative to that of MCM-41 (Figure 3). Similar results were obtained for the Gd-containing materials (not shown here). The intensities of all the Bragg peaks are reduced to the extent that the (110) and (200) reflections are either absent or very weak. Although a loss of structural order could be the cause of this change, it is more likely that the introduction of the bulky $Eu(nta)_3$ fragment inside the channels of the support affects the peak intensities by reducing the X-ray scattering contrast between the silica framework and pore-filling material.[7a,13]

The texture properties were calculated from the nitrogen adsorption isotherms measured at 77 K (not shown), and are given in Table 1. Unmodified MCM-41 exhibits a reversible type IV isotherm, characteristic of mesoporous materials according to the IUPAC classification.[14] A sharp capillary condensation/evaporation step, which is related to the volume of pore space confined by adsorbate film on the pore walls, appears in the relative pressure (p/p_0) range of 0.25–0.35, and the pore size distribution (PSD) curve is quite narrow with a full width at half maximum (fwhm) of about 0.45 nm, which reflects the uniform pore size. The S_{BET}, V_p and d_p values lie within the expected ranges for this type of ordered mesoporous silica (Table 1).[15] A reversible type IV isotherm was also recorded for MCM-41-pyr (**1**), although in comparison with MCM-41, the capillary condensation step is less sharp, which indicates an inflection point at a lower p/p_0 coordinate, and a major decrease in S_{BET}, V_p and d_p occurs (Table 1). The fwhm of the PSD curve is similar to that for MCM-41. These results are in agreement with the powder XRD data and indicate that the regular mesoporous structure of the support was preserved and that tespyr was successfully grafted on the internal surface. By using the method reported by Zhao et al. for the fast calculation of molecular volumes,[16] the van der Waals volume occupied by one anchored ligand in **1** (with one residual ethoxy group per organosilane group) is estimated to be 250 $Å^3$. It follows that the theoretical V_p for **1** is 0.48 $cm^3 g^{-1}$ (based on an initial specific total pore volume of 0.81 $cm^3 g^{-1}$ for MCM-41 and a final ligand loading of 0.93 $mmol g^{-1}$), which is somewhat higher than the experimentally determined volume of 0.33 $cm^3 g^{-1}$. S_{BET}, V_p and d_p values decrease further after treatment of **1** with $Eu(nta)_3(H_2O)_2$ to give **2a**. The capillary condensation step is poorly defined and the PSD curve is broader, with an fwhm that is approximately double that for **1**. On the basis of a molecular volume of 1000 $Å^3$ for the $Eu(nta)_3(H_2O)$ fragment, a V_p of 0.33 $cm^3 g^{-1}$ for **1**, and a final Eu loading of 0.05 $mmol g^{-1}$, the theoretical V_p for **2a** is 0.28 $cm^3 g^{-1}$, which is, again, slightly higher than the measured value of 0.2 $cm^3 g^{-1}$ (Table 1). The discrepancies between the experimental and theoretical specific total pore volumes for **1** and **2a** may mean that some of the organic ligands (and subsequently Eu complexes) are located at the pore entrances, which results in partial pore blockage. Treatment of **2a** with pyridine or mpso in chloroform leads to an increase in S_{BET}, V_p and d_p, and a narrower PSD curve, which is consistent with the partial leaching of the tris-β-diketonate complexes. We may speculate that pore blocking effects are reduced by preferential dissolution of $Eu(nta)_3$ species complexed or weakly adsorbed at the pore entrances.

Table 1. Texture properties of the silica and hybrid materials.

Sample	S_{BET} ($m^2 g^{-1}$)[a]	V_p ($cm^3 g^{-1}$)[b]	d_p (nm)[c]
MCM-41	1056	0.81	3.6
1	568	0.33	3.0
2a	437	0.20	2.4
3a	556	0.27	2.6
4a	527	0.27	2.6

[a] BET specific surface area calculated for p/p_0 between 0.03 and 0.15. [b] Specific total pore volume calculated from the volume of N_2 adsorbed at $p/p_0 \approx 0.96$. [c] Mode pore width calculated by the BJH method applied to the adsorption branch of the isotherm.

The lanthanide-containing materials were further characterised by FTIR and FT Raman spectroscopy. The FTIR spectra are dominated by the bands of the MCM-41 framework in the region 450–1250 cm^{-1}; weaker bands due to the tethered pyr ligand are observed between 1350 and 1700 cm^{-1} (Supporting Information). In the range 550–1650 cm^{-1}, the Raman spectra are more informative with respect to the immobilised metal complexes, being well described by the sum of the spectra of MCM-41-pyr and $Ln(nta)_3(H_2O)_2$, with only small frequency and/or intensity changes. Figure 4 shows a comparison of the spectra of $Eu(nta)_3(H_2O)_2$ and the materials **1**, **2a** and **4a**. The relative intensities of several bands due to the $Eu(nta)_3$ fragment (see, for example, the absorption bands at 1383, 1470 and 1628 cm^{-1}) decrease slightly on going from **2a** to **4a**. For materials **3a** and **4a** (and **3b** and **4b**), bands arising from pyridine or mpso could not be observed, which is not unexpected since in the spectra of complexes **5** and **6**, the bands from these two ligands are considerably weaker than those from the $Eu(nta)_3$ fragment. Additionally, for materials **3a** and **3b**, bands due to coordinated pyridine molecules appear in the region dominated by the bands of the tethered pyr ligand.

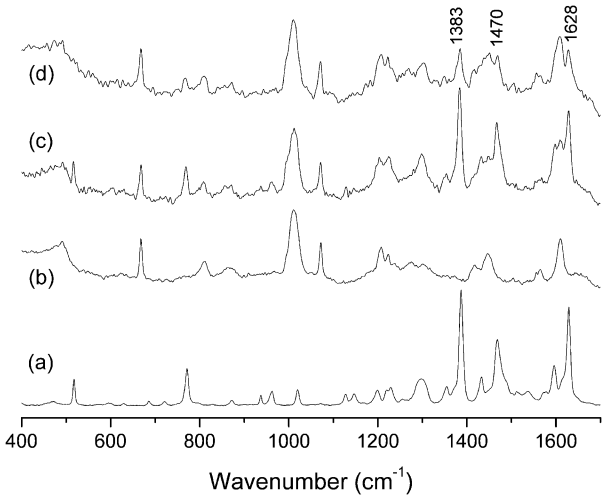

Figure 4. Raman spectra in the range 400–1700 cm^{-1} for (a) $Eu(nta)_3(H_2O)_2$, (b) MCM-41-pyr (**1**), (c) $Eu(nta)_3(H_2O)$(MCM-41-pyr) (**2a**) and (d) $Eu(nta)_3$(mpso)(MCM-41-pyr) (**4a**).

Photoluminescence Studies

The absorption spectrum of unmodified MCM-41 displays two absorption edges at about 258 and 340 nm (Figure 5). These components are detected in the spectrum of MCM-41-pyr (**1**) with a reduction in the fwhm of the absorption band at 258 nm and a decrease in the relative intensity of the component at 340 nm, which may be ascribed to the chemical modification of the silica support. For the Eu^{3+}-containing materials, the absorption peak related to MCM-41 remains unaltered, and an intense component appears at about 330 nm, which is ascribed to the excited states of the organic ligands (Figure 5). The fwhm of this component is different for each material, which may be due in part to the influence of the different Eu^{3+}-coordinated ligands L′ (H_2O, py or mpso) present.

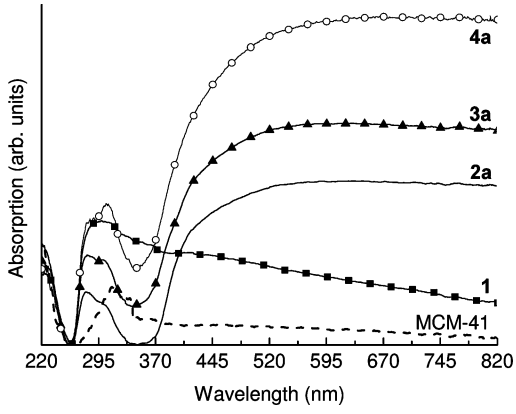

Figure 5. Room-temperature absorption spectra of MCM-41, MCM-41-pyr (**1**), $Eu(nta)_3(H_2O)$(MCM-41-pyr) (**2a**), $Eu(nta)_3$(py)(MCM-41-pyr) (**3a**) and $Eu(nta)_3$(mpso)(MCM-41-pyr) (**4a**).

Figure 6A shows the excitation spectra of **2a**, **3a** and **4a** monitored within the Eu^{3+} intra-$4f^6$ $^5D_0 \rightarrow {}^7F_2$ transition. All of the spectra display a large broad band peaking at 330 nm (as observed in the absorption spectra) with an fwhm of 11700 cm^{-1} for **2a**, 8400 cm^{-1} for **3a** and 7700 cm^{-1} for **4a**. The absence of Eu^{3+} intra-$4f^6$ lines indicates that in all the materials the Eu^{3+} ions are sensitised through the ligands, rather than by direct intra-$4f^6$ excitation. At 14 K, apart from a small reduction (10%) in the fwhm, the spectra resemble those acquired at room temperature (not shown here).

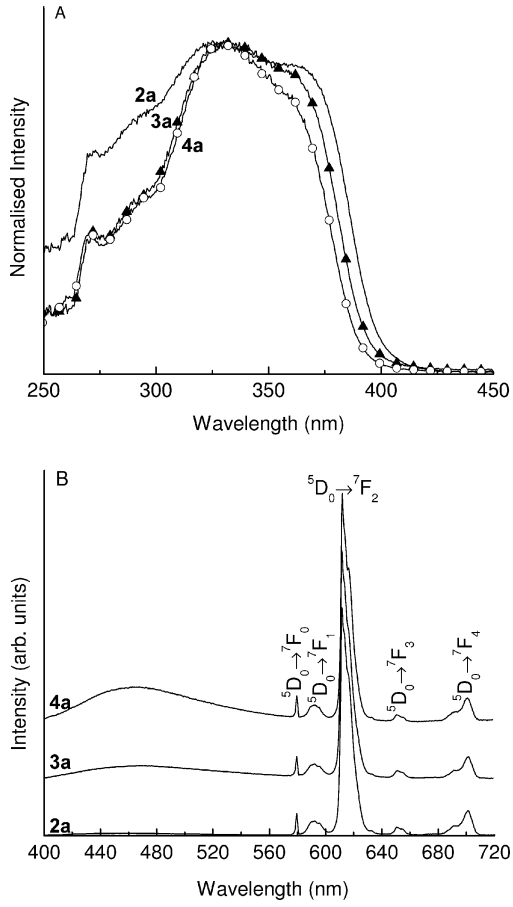

Figure 6. Room-temperature (A) excitation spectra monitored at 612 nm and (B) emission spectra excited at 380 nm of $Eu(nta)_3(H_2O)$(MCM-41-pyr) (**2a**), $Eu(nta)_3$(py)(MCM-41-pyr) (**3a**) and $Eu(nta)_3$(mpso)(MCM-41-pyr) (**4a**).

The excitation spectra of complexes **5** and **6** monitored within the Eu^{3+} intra-$4f^6$ $^5D_0 \rightarrow {}^7F_2$ transition display a large broad band with one component at about 320 nm and a more intense feature centred at 400 nm for **6** and 420 nm for **5**, which is ascribed to the excited states of the ligands (Figure 7A). A series of Eu^{3+} intra-$4f^6$ lines ascribed to the $^7F_{0,1} \rightarrow {}^5D_{2,1}$ transitions are also present. The relatively high intensities of these lines indicate that the Eu^{3+} ions are excited by the excited states of the ligands and through direct excitation into the intra-$4f^6$ levels. Comparing these results with those of the supported materials (Figure 6A), we may conclude that the sensitisation of the Eu^{3+} ions is better for the immobilised mixed-ligand complexes. The significant changes observed for the ligand excited states, namely in their energy and fwhm, can be ascribed to an effective interaction between the complexes and the hybrid host.

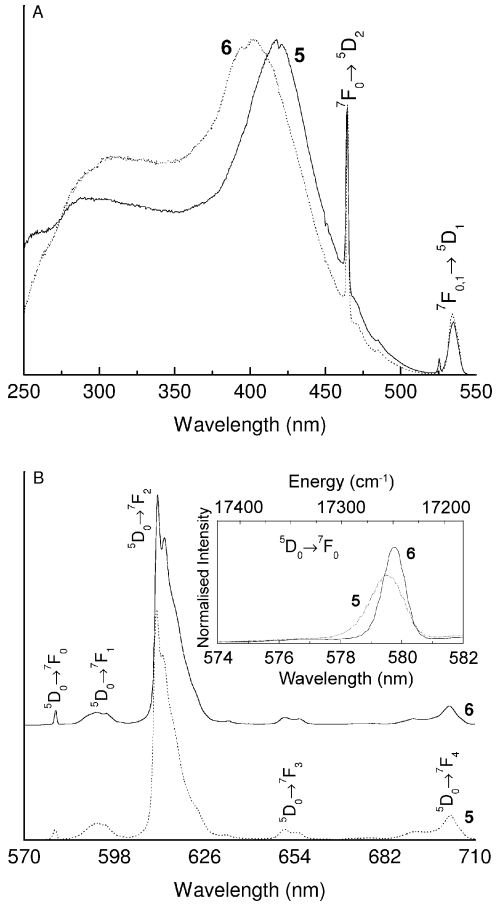

Figure 7. Room-temperature (A) excitation spectra monitored at 612 nm and (B) emission spectra of $Eu(nta)_3(py)_2$ (**5**) and $Eu(nta)_3(mpso)_2$ (**6**) excited at 400 and 420 nm, respectively. The $^5D_0 \rightarrow {}^7F_0$ transition is magnified in the inset.

Figure 6B shows the room temperature emission spectra of **2a**, **3a** and **4a** obtained with an excitation wavelength of 380 nm. The emission for all the materials displays the typical $^5D_0 \rightarrow {}^7F_{0-4}$ Eu^{3+} transitions and a low-intensity broad band peaking at 450 nm. The excitation wavelength was varied along the Eu^{3+} excitation spectra (Figure 6A) and, apart from a decrease in the relative intensity of the broad band, the energy, number of components and fwhm of the intra-$4f^6$ lines remained unaltered, which indicates that all of the Eu^{3+} ions occupy the same average local environment within each sample. The large broad band, most evident for **4a**, may arise either from the excited states of the ligands or from the MCM-41 host, which is a visible broad band emitter with a lifetime value in the 10–100 ns range.[17] In order to shed light on the origin of this band, the emission of the corresponding $Gd(nta)_3(L')$(MCM-41-pyr) materials (**2b**–**4b**) was characterised. Figure 8 shows the emission spectra of **2b** (L′ = H_2O) acquired at 14 K. The spectra display a broad band with three main components at 515, 550 and 590 nm (19418, 18182 and 16950 cm^{-1}, respectively) and a weaker component at 450 nm. At room temperature, the emission spectrum is dominated by the latter component (inset of Figure 8). The three main peaks can be ascribed to a resolvable vibrational fine structure originating from a single triplet state; the energetic separation between them is about 1235 cm^{-1}, which corresponds approximately to a vibrational progression typical of the π–π* emission of aromatic molecules.[18] Moreover, the timescale behind these emissions lies in the millisecond time domain, whereas the timescale of the weaker component at 450 nm is faster (beyond the detection limits of 10^{-5} s for our equipment), as the time-resolved emission spectrum in Figure 8 demonstrates for **2b**.

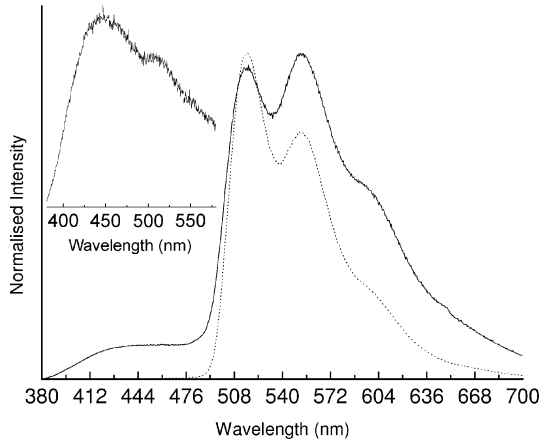

Figure 8. Low-temperature (14 K) emission spectra of $Gd(nta)_3(H_2O)$(MCM-41-pyr) (**2b**) excited at 300 nm in steady-state (solid line) and time-resolved mode (dashed line, starting delay = 0.05 ms, integration window = 20.00 ms). The inset shows the room-temperature emission excited at 300 nm.

The lifetime of the triplet state was estimated by monitoring the emission decay curve at 515 nm under a 370-nm excitation wavelength (not shown here). By assuming a single exponential decay curve, a lifetime value of 5.92 ± 0.05 ms was found, which reinforces the triplet nature of the emission. It follows that the weaker component at 450 nm for the gadolinium-and europium-containing materials may be tentatively attributed to the intrinsic MCM-41 emission.

With the goal of obtaining further insight into the Eu^{3+} local coordination environments in the different materials and into the effects of incorporation into the modified MCM-41 host, we scanned the emission spectra at a higher resolution at 14 K. The relative intensity of the ligand band is reduced by about 10% (not shown here). As found in the room temperature measurements, the energy, fwhm and relative intensity of the Eu^{3+} emission lines were found to be independent of the excitation wavelength, which confirms that all of the Eu^{3+} ions occupy the same average local environment within each sample. Figure 9 shows in detail the Eu^{3+} emission lines for **2a**, **3a** and **4a** under excitation at 330 nm. The maximum splitting of the $^5D_0 \rightarrow {}^7F_{1,2}$ transitions into 3 and 5 Stark components, respectively, indicates that the Eu^{3+} local environments in all three materials have low symmetry without an inversion centre, in accordance with the higher relative intensity of the $^5D_0 \rightarrow {}^7F_2$ transition. A comparison of the three spectra reveals differences in the energy and relative intensity of the emission lines, which points to a modification of the Eu^{3+} first coor-

dination shell. To probe the nature of these structural changes, it is important to quantify the energy (E_{0-0}) of the nondegenerate $^5D_0 \rightarrow {}^7F_0$ transition, since this transition is usually related to the covalency degree of the first coordination shell of Eu^{3+}.[19a–19c] The peak energies of the $^5D_0 \rightarrow {}^7F_0$ transition are 17244.4 cm^{-1} for **2a**, 17247.8 cm^{-1} for **4a** and 17250.3 cm^{-1} for **3a**. The blueshift of the E_{0-0} lines for **3a** and **4a** with respect to that for **2a** suggests that in the former materials the Eu^{3+} ions experience a less covalent local environment.[19b,19c] This assumption is based on the fact that the energy of the $^5D_0 \rightarrow {}^7F_0$ transition is related to the so-called nephelauxetic effect, in which the redshift observed for d–d and f–f energy differences, with respect to the free ion, is related to a decrease in the values of the Slater integrals and spin–orbit coupling parameter.[19b–19e] The less covalent environments in **3a** and **4a** may be induced by changes in the Eu^{3+} first neighbours and/or an increase in the average europium(III)–ligand distance. The replacement of the water molecule by the organic ligands may induce a lengthening of the average Eu–O distance and a less covalent Eu–O bond.

As shown in Figure 9, the emission features of **3a** and **4a** are comparable with those of complexes **5** and **6** (Figure 7B), especially with respect to the number of Stark components and their relative intensities, as well as the energy of the $^5D_0 \rightarrow {}^7F_0$ transition. This substantiates the immobilisation of complexes of the type $Eu(nta)_3(L')(L'')$. The fwhm of the $^5D_0 \rightarrow {}^7F_0$ line is larger for **3a** and **4a**, which suggests a broader distribution of similar Eu^{3+} local coordination environments.

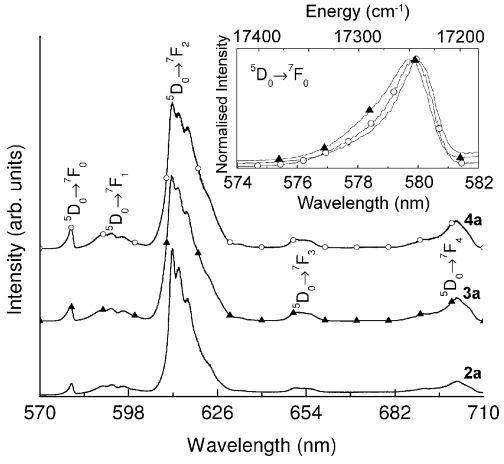

Figure 9. Low-temperature (14 K) Eu^{3+} emission spectra of $Eu(nta)_3(H_2O)$(MCM-41-pyr) (**2a**), $Eu(nta)_3$(py)(MCM-41-pyr) (**3a**) and $Eu(nta)_3$(mpso)(MCM-41-pyr) (**4a**), excited at 330 nm. The $^5D_0 \rightarrow {}^7F_0$ transition is magnified in the inset.

The $^5D_0$ lifetimes of **2a**, **3a** and **4a** were measured under excitation at 330 nm in the temperature interval 14–300 K. For complexes **5** and **6**, the emission decay curves were acquired at 300 K under direct excitation into the $^5D_1$ level (534 nm). All of the decay curves were well reproduced by a single exponential function, and the lifetime values listed in Table 2 were obtained. The higher values measured for **3a** and **4a** than that for **2a** are consistent with the replacement of the europium(III)-coordinated water molecule in **2a** with either pyridine (**3a**) or mpso (**4a**). However, the values for **3a** and **4a** are lower than those estimated for complexes **5** and **6**. The possibility that the lower $^5D_0$ lifetimes for the supported complexes arise from having higher nonradiative transition probabilities will be addressed next.

By using the methods described in more detail elsewhere,[7a] where only nonradiative and radiative processes are assumed to essentially be involved in the depopulation of the excited state, the radiative (k_r) and nonradiative (k_{nr}) transition probabilities and the $^5D_0$ quantum efficiencies were estimated for the supported materials **2a**, **3a** and **4a** and for complexes **5** and **6** (Table 2). The higher $^5D_0$ quantum efficiency for **3a** (29.9%) than that for **2a** (24.8%) arises from an increase in k_r and a decrease in k_{nr}. The decrease in the last parameter is in good agreement with the removal of water molecules from the first coordination sphere of Eu^{3+}. Although **4a** presents an even lower k_{nr} value, the $^5D_0$ quantum efficiency is slightly lower than that for **3a**, which is accounted for by the lower k_r value. The quantum efficiency estimated for **3a** is only slightly lower than that estimated for complex **5**, which can be considered as a model for the desired supported species. The difference in the values can be attributed to a slightly lower k_r value combined with a slightly higher k_{nr} value for **3a**. Complex **6**, with two mpso ligands in the first coordination sphere, has a high quantum efficiency of 51.9%, which is evidently related to the comparatively high k_r and low k_{nr} values.

The photoluminescence features of the europium-containing supported materials were further quantified by estimating the absolute emission quantum yields. The maximum values for all three materials were obtained by using an excitation wavelength of 330 nm. Material **2a** exhibits the highest value of 12%, which indicates that the removal

Table 2. Room-temperature $^5D_0$ lifetime values, radiative and nonradiative transition probabilities, $^5D_0$ quantum efficiency and absolute emission quantum yields for the compounds. The lifetime values in parentheses were acquired at 14 K. The excitation wavelength was 330 nm for **2a**–**4a** and 534 nm for **5** and **6**.

	$Eu(nta)_3(L')$(MCM-41-pyr)			$Eu(nta)_3(L')_2$	
	2a	**3a**	**4a**	**5**	**6**
τ (ms)	0.276 ± 0.002 (0.499 ± 0.004)	0.313 ± 0.001 (0.650 ± 0.001)	0.336 ± 0.001 (0.690 ± 0.001)	0.350 ± 0.001	0.468 ± 0.001
k_r (ms^{-1})	0.898	0.956	0.777	0.976	1.108
k_{nr} (ms^{-1})	2.725	2.239	1.952	1.901	1.028
q (%)	24.8	29.9	28.5	33.5	51.9
ϕ (%)	12.0	7.0	7.0	–	–

of the water molecules by introduction of organic ligands induces the presence of extra nonradiative channels.

Conclusions

In the present work, we have shown that the silane coupling agent tespyr can readily be prepared and used to functionalise the ordered mesoporous silica MCM-41 with pyridyl groups. A luminescent material was subsequently prepared by immobilisation of $Eu(nta)_3(H_2O)_2$ complexes in the organic–inorganic hybrid. The possibility to further modify the luminescence properties of this material by replacement of residual coordinated water molecules by other groups has been demonstrated for the ligands pyridine and methyl phenyl sulfoxide. By comparison with the photoluminescence results for the complexes $Eu(nta)_3(py)_2$ and $Eu(nta)_3(mpso)_2$, it is clear that the interaction between the host and guest has a strong effect on the excited states of the organic ligands, and the sensitisation of the Eu^{3+} ions seems to be better. Although the substitution of coordinated water molecules by pyridine or mpso leads to an increase in the $^5D_0$ lifetime (from 0.28 to 0.31–0.34 ms) and the quantum efficiency (from 25 to 28–30%) measured at room temperature, the absolute emission quantum yield decreases from 12 to 7%, which indicates the presence of extra nonradiative channels. Owing to the bulky nature of the $Ln(nta)_3$ fragment, the lanthanide loadings in the supported materials are limited to less than 1 wt.-%, and only about 6% of the pendant monodentate ligands is coordinated to the Ln^{3+} centres. Future work could be directed at improving this situation by using a support with a larger pore volume and size.

Experimental Section

Characterisation: Microanalyses for CHN and ICP-AES determination of Eu and Gd were performed at the University of Aveiro. Thermogravimetric analyses (TGA) were carried out under a static atmosphere of air with a Shimadzu TGA-50 system at a heating rate of 5 K min^{-1}. Powder XRD data were collected on an X′Pert MPD Philips diffractometer, equipped with an X′Celerator detector, a curved graphite monochromator (Cu-K_α X-radiation, λ = 1.54060 Å) and a flat-plate sample holder, in a Bragg–Brentano para-focusing optics configuration (40 kV, 50 mA). Samples were step-scanned with 0.02° 2θ steps with a counting time of 2 s per step. The N_2 adsorption–desorption isotherms were measured at 77 K by using a gravimetric adsorption apparatus equipped with a CI electronic MK2–M5 microbalance and an Edwards Barocel pressure sensor. Prior to the analyses, the samples were treated in vacuo overnight, at 573 K for MCM-41 and 323 K (to minimize degradation of the immobilized species) for the hybrid organic–inorganic materials.

FTIR spectra were obtained by using a FTIR Mattson-7000 infrared spectrophotometer with 2 cm^{-1} resolution. FT Raman spectra were recorded on a RFS-100/S Bruker FT-spectrometer, by using an Nd:YAG laser (Coherent compass-1064/500) with an excitation wavelength of 1064 nm and 2 cm^{-1} resolution. Solution ^{1}H- and ^{13}C NMR spectra were measured with a Bruker CXP 300 spectrometer. Solid-state magic-angle-spinning (MAS) NMR spectra were recorded at 79.49 MHz for ^{29}Si and 125.76 MHz for ^{13}C on Bruker Avance 400/500 spectrometers. ^{29}Si CP MAS NMR spectra were recorded with 4.0 μs ^{1}H 90° pulses, 8 ms contact time with a spinning rate of 5 kHz and 5 s recycle delays. ^{13}C CP MAS NMR spectra were recorded with 4.5 μs ^{1}H 90° pulses and 2 ms contact time with a spinning rate of 7.0 kHz and 4 s recycle delays.

The absorption spectra were recorded at room temperature with a Jasco V-560 UV/Vis spectrophotometer. The photoluminescence spectra were recorded between 14 K and room temperature on a Fluorolog-3 Model FL3–2T spectrometer with double excitation and a TRIAX 320 single emission spectrometer coupled to a R928 photomultiplier, by using a front face acquisition mode. The excitation source was a 450 W Xenon lamp. Emission was corrected for the spectral response of the monochromators and the detector by using the typical correction spectrum provided by the manufacturer, and the excitation spectra were corrected for the spectral distribution of the lamp intensity by using a photodiode reference detector. The emission decay curves were acquired between 14 K and room temperature with the setup described above by using a pulsed Xe–Hg lamp (6-μs pulse at half width and 20–30 μs tail). The absolute emission quantum yields were measured at room temperature by using a Quantum Yield Measurement System C9920–02 from Hamamatsu with a 150 W Xenon lamp coupled to a monochromator for wavelength discrimination, an integrating sphere as sample chamber and a multichannel analyzer for signal detection.

Synthesis

Materials and Methods: All preparations and manipulations were carried out by using standard Schlenk techniques under nitrogen. Solvents (toluene, *n*-hexane, CH_2Cl_2 and $CHCl_3$) were purchased from Aldrich and dried by standard procedures, distilled under nitrogen and kept over 4-Å molecular sieves. Pyridine (py, Baker), europium(III) chloride hexahydrate, gadolinium(III) chloride hexahydrate, 1-(2-naphthoyl)-3,3,3-trifluoroacetone, ethyl 4-pyridylacetate (epa), 3-triethoxysilylpropylamine (tespa) and methyl phenyl sulfoxide (mpso) (all Aldrich) were purchased from commercial sources and used as received. Literature procedures were used to prepare $Ln(nta)_3(H_2O)_2$ (Ln = Eu, Gd).[20] Purely siliceous MCM-41 was synthesised as described previously with $[CH_3(CH_2)_{13}N(CH_3)_3]Br$ as the templating agent.[21] The surfactant template was removed by calcination at 833 K under air for 6 h. Powder XRD (*hkl* in parentheses): 2θ [°] = 2.65 (100), 4.49 (110), 5.16 (200), 6.75 (210); $a = 2d_{100}/\sqrt{3}$ = 38.50 Å.

3-Triethoxysilylpropyl 4-Pyridylacetamide (tespyr): epa (0.75 g, 4.54 mmol) was added to tespa (1.00 g, 4.54 mmol), and the resultant mixture was stirred for 48 h at 393 K under nitrogen. The ethanol formed was removed under reduced pressure to yield tespyr as an orange oil, which was used without further purification. FTIR (KBr): $\tilde{\nu}$ = 3291 (m), 3070 (m), 3032 (m), 2974 (s), 2927 (s), 2886 (s), 1677 (sh), 1650 (s), 1600 (m), 1561 (m), 1442 (m), 1416 (w), 1390 (w), 1366 (w), 1346 (w), 1326 (m), 1297 (m), 1269 (m), 1228 (m), 1194 (m), 1166 (m), 1124 (sh), 1102 (vs), 1078 (vs), 994 (w), 958 (m), 898 (m), 794 (m), 777 (m) cm^{-1}. ^{1}H NMR (300 MHz, 298 K, $CDCl_3$, TMS): δ = 8.53 (d, 2 H, H^2, H^6), 7.23 (d, 2 H, H^3, H^5), 6.59 (br., 1 H, NH), 3.80 (q, 6 H, H^{11}), 3.52 (s, 2 H, H^7), 3.24 (m, 2 H, H^8), 1.60 (m, 2 H, H^9), 1.23 (t, 9 H, H^{12}), 0.60 (m, 2 H, H^{10}) (see Scheme 1 for the atom numbering) ppm. ^{13}C NMR (75.48 MHz, 298 K, $CDCl_3$, TMS): δ = 168.9 (C=O), 149.7 (C^2, C^6), 144.2 (C^4), 124.4 (C^3, C^5), 58.2 (C^{11}), 42.7 (C^7), 41.9 (C^8), 22.6 (C^9), 18.1 (C^{12}), 7.5 (C^{10}) ppm.

MCM-41-pyr (1): After removal of physisorbed water from calcined MCM-41 by heating at 453 K under reduced pressure for 2 h, a solution of tespyr (ca. 5 mmol) in toluene (5 mL) was added to

a suspension of MCM-41 (1.5 g) in toluene (30 mL), and the mixture was stirred under reflux for 24 h. The resultant powder was filtered, washed with dichloromethane (3 × 30 mL) and dried under reduced pressure at room temperature. C 10.41, H 3.02, N 2.61%. FTIR (KBr): $\tilde{\nu}$ = 2929 (w), 1637 (m), 1559 (w), 1424 (w), 1234 (sh), 1199 (sh), 1081 (vs), 963 (m), 800 (m), 675 (vw), 544 (w), 458 (s) cm^{-1}. Raman: $\tilde{\nu}$ = 3066 (vs), 2933 (vs), 2896 (vs), 1610 (s), 1565 (m), 1447 (s), 1417 (m), 1301 (m), 1275 (m), 1223 (m), 1208 (sh), 1072 (s), 1011 (s), 863 (m), 812 (m), 668 (s), 622 (w), 491 (m) cm^{-1}. ^{13}C CP MAS NMR: δ = 171.0 (C=O), 147.8 (C^2, C^6, C^4), 124.7 (C^3, C^5), 58.4 (C^{11}), 41.7 (C^7, C^8), 22.0 (C^9), 9.1 (C^{10}) ppm. ^{29}Si CP MAS NMR: δ = –57.9 (T^2), –64.5 (T^3), –102.5 (Q^3), –109.9 (Q^4) ppm.

Ln(nta)$_3$(H$_2$O)(MCM-41-pyr) [Ln = Eu (2a), Gd (2b)]: A solution of Ln(nta)$_3$(H$_2$O)$_2$ (0.59 mmol) in $CHCl_3$ (30 mL) was added to a suspension of MCM-41-pyr (0.60 g) in $CHCl_3$ (30 mL), and the mixture was stirred at room temperature for either 24 h (Eu) or 42 h (Gd). The solid was then filtered, washed several times with $CHCl_3$ and dried under reduced pressure. **2a:** C 11.10, H 3.13, N 2.51, Eu 0.75%. FTIR (KBr): $\tilde{\nu}$ = 2946 (w), 1642 (m), 1564 (w), 1425 (w), 1235 (s), 1196 (sh), 1078 (vs), 963 (m), 797 (m), 684 (vw), 554 (w), 458 (s) cm^{-1}. Raman: $\tilde{\nu}$ = 3414 (s), 3063 (s), 2928 (s), 2895 (s), 1628 (m), 1609 (m), 1597 (m), 1567 (vw), 1467 (m), 1484 (m), 1432 (m), 1383 (s), 1354 (w), 1298 (m), 1224 (m), 1203 (m), 1128 (w), 1071 (m), 1012 (m), 961 (w), 936 (vw), 871 (w), 856 (w), 808 (w), 769 (m), 668 (m), 516 (m) cm^{-1}. **2b:** C 11.15, H 2.52, N, 2.45, Gd 0.85%. FTIR (KBr): $\tilde{\nu}$ = 1645 (m), 1558 (w), 1540 (w), 1453 (w), 1422 (w), 1233 (s), 1197 (sh), 1080 (vs), 963 (m), 803 (m), 577 (vw), 458 (m) cm^{-1}. Raman: $\tilde{\nu}$ = 3414 (s), 3063 (s), 2933 (s), 2896 (sh), 1628 (m), 1611 (m), 1468 (w), 1442 (w), 1384 (m), 1301 (w), 1222 (w), 1205 (w), 1171 (m), 1010 (m), 866 (w), 806 (w), 769 (w), 668 (w), 516 (w) cm^{-1}.

Ln(nta)$_3$(py)(MCM-41-pyr) [Ln = Eu (3a), Gd (3b)]: Pyridine (3.0 mL) was added to a suspension of Ln(nta)$_3$(H$_2$O)(MCM-41-pyr) (0.30 g) in $CHCl_3$ (30 mL), and the mixture was stirred at room temperature for either 16 h (Eu) or 22 h (Gd). The solid was then filtered, washed several times with $CHCl_3$ (20 mL) and dried under reduced pressure. **3a:** Eu 0.50%. FTIR (KBr): $\tilde{\nu}$ = 2943 (vw), 1636 (m), 1559 (w), 1425 (w), 1382 (w), 1232 (s), 1196 (sh), 1079 (vs), 963 (m), 801 (m), 545 (vw), 458 (s) cm^{-1}. Raman: $\tilde{\nu}$ = 3412 (s), 3064 (s), 2934 (s), 2895 (sh), 1630 (m), 1608 (m), 1565 (w), 1467 (m), 1447 (m), 1383 (m), 1298 (m), 1223 (m), 1205 (m), 1072 (m), 1012 (m), 997 (m), 864 (w), 810 (w), 767 (w), 668 (m), 490 (w) cm^{-1}. **3b:** Gd 0.55%. FTIR (KBr): $\tilde{\nu}$ = 2943 (vw), 1636 (m), 1559 (w), 1424 (w), 1384 (w), 1234 (s), 1202 (sh), 1081 (vs), 963 (m), 804 (m), 545 (vw), 458 (s) cm^{-1}. Raman: $\tilde{\nu}$ = 3415 (s), 3065 (sh), 2932 (sh), 1604 (m), 1554 (w), 1445 (w), 1383 (w), 1223 (w), 1204 (w), 1071 (m), 1009 (m), 848 (w), 803 (w), 768 (w), 667 (m), 490 (w) cm^{-1}.

Ln(nta)$_3$(mpso)(MCM-41-pyr) [Ln = Eu (4a), Gd (4b)]: mpso (0.1 g, 0.71 mmol) was added to a suspension of Ln(nta)$_3$(H$_2$O)(MCM-41-pyr) (0.10 g) in $CHCl_3$ (10 mL), and the mixture was stirred at room temperature for either 23 h (Eu) or 26 h (Gd). The solid was then filtered, washed several times with $CHCl_3$ (3 × 20 mL) and dried under reduced pressure. **4a:** Eu 0.72%. FTIR (KBr): $\tilde{\nu}$ = 2943 (vw), 1641 (m), 1561 (w), 1426 (w), 1381 (w), 1356 (w), 1234 (s), 1200 (sh), 1082 (vs), 964 (m), 797 (m), 679 (w), 544 (sh), 461 (s) cm^{-1}. Raman: $\tilde{\nu}$ = 3412 (s), 3063 (s), 2932 (s), 2896 (s), 2857 (m), 2811 (m), 2727 (m), 1629 (m), 1610 (m), 1596 (m), 1561 (w), 1470 (m), 1446 (m), 1383 (m), 1298 (m), 1224 (m), 1207 (m), 1071 (m), 1010 (m), 995 (sh), 807 (w), 770 (w), 667 (m), 479 (vw) cm^{-1}. **4b:** Gd 0.75%. FTIR (KBr): $\tilde{\nu}$ = 2946 (vw), 1642 (m), 1563 (w), 1425 (w), 1343 (sh), 1235 (s), 1200 (sh), 1080 (vs), 963 (m), 799 (m), 683 (vw), 548 (vw), 458 (s) cm^{-1}. Raman: $\tilde{\nu}$ = 3418 (vs), 3063 (s), 2930 (s), 1630 (m), 1610 (m), 1467 (m), 1384 (m), 1072 (w), 1009 (m), 668 (w) cm^{-1}.

Eu(nta)$_3$(py)$_2$ (5): Pyridine (0.6 mL) was added to a solution of Eu(nta)$_3$(H$_2$O)$_2$ (0.86 g, 0.88 mmol) in $CHCl_3$ (40 mL) at room temperature, and the mixture was stirred for 6 h. After evaporation of the solvents to dryness, the resultant solid was washed with *n*-hexane (3 × 20 mL) and dried under reduced pressure. Yield: 0.74g, 75%. $C_{52}H_{34}EuF_9N_2O_6$ (1105.80): calcd. C 56.48, H 3.10, N 2.53; found C 56.05, H 3.08, N 2.17. FTIR (KBr): $\tilde{\nu}$ = 3058 (m), 1612 (vs), 1569 (s), 1531 (s), 1461 (m), 1386 (m), 1353 (m), 1297 (vs), 1251 (m), 1220 (m), 1197 (s), 1133 (vs), 1072 (m), 958 (m), 935 (m), 865 (m), 823 (m), 792 (s), 765 (m), 748 (m), 701 (m), 684 (s), 620 (m), 568 (m), 518 (m), 470 (m), 420 (vw), 395 (m), 352 (m) cm^{-1}. Raman: $\tilde{\nu}$ = 3059 (m), 1629 (vs), 1595 (m), 1572 (w), 1533 (w), 1511 (w), 1468 (s), 1432 (m), 1386 (vs), 1354 (m), 1297 (m), 1254 (w), 1228 (m), 1218 (m), 1198 (m), 1147 (m), 1127 (m), 1071 (vw), 1036 (w), 1019 (m), 1006 (m), 962 (m), 937 (m), 871 (w), 828 (vw), 771 (m), 721 (w), 685 (w), 652 (vw), 629 (vw), 592 (vw), 517 (vw), 468 (m), 393 (w), 308 (m), 229 (w), 193 (w), 105 (m) cm^{-1}. ^1H NMR (300 MHz, 298 K, $CDCl_3$, TMS): δ = 13.35 (br., 4 H, py-H_α), 9.15 (t, 2 H, py-H_γ), 8.79 (br., 4 H, py-H_β), 8.7–7.0 (series of broad peaks and multiplet signals, 21 H, naphth.), 2.94 (s, 3 H, CH) ppm.

Eu(nta)$_3$(mpso)$_2$ (6): A solution of mpso (0.23 g, 1.62 mmol) in $CHCl_3$ (2 mL) was added to a solution of Eu(nta)$_3$(H$_2$O)$_2$ (0.8 g, 0.81 mmol) in $CHCl_3$ (40 mL) at room temperature, and the mixture was stirred for 8 h. After evaporation of the solvents to dryness, the resultant oil was washed with *n*-hexane (3 × 20 mL) and dried under reduced pressure. Yield: 0.70 g, 70%. $C_{56}H_{40}EuF_9S_2O_8$ (1227.99): calcd. C 54.77, H 3.28, S 5.22; found C 54.24, H 3.74, S 5.81. FTIR (KBr): $\tilde{\nu}$ = 3057 (m), 3019 (sh), 2919 (w), 1614 (vs), 1594 (m), 1570 (s), 1531 (s), 1509 (s), 1478 (m), 1462 (m), 1444 (w), 1430 (w), 1384 (m), 1353 (m), 1297 (vs), 1249 (m), 1226 (m), 1197 (s), 1186 (s), 1134 (vs), 1091 (m), 1073 (m), 1048 (m), 1017 (m), 997 (w), 958 (m), 936 (m), 918 (w), 900 (w), 865 (m), 823 (m), 790 (s), 766 (m), 746 (m), 721 (w), 683 (s), 623 (w), 568 (m), 518 (m), 500 (m), 472 (m), 395 (w), 347 (w) cm^{-1}. Raman: $\tilde{\nu}$ = 3059 (m), 3015 (w), 2918 (w), 1629 (vs), 1595 (m), 1511 (w), 1467 (s), 1432 (m), 1386 (vs), 1354 (m), 1296 (m), 1253 (vw), 1228 (m), 1218 (m), 1199 (m), 1147 (m), 1128 (m), 1092 (vw), 1020 (m), 999 (m), 962 (m), 937 (w), 870 (w), 771 (m), 722 (w), 684 (m), 614 (vw), 591 (vw), 518 (m), 466 (vw), 394 (w), 309 (vw), 229 (w), 194 (w), 105 (m) cm^{-1}. ^1H NMR (300 MHz, 298 K, CD_2Cl_2, TMS): δ = 9.51 (br., 4 H, phenyl-H_α), 8.8–6.4 (series of broad peaks and multiplet signals, 27 H, phenyl-$H_{\beta,\gamma}$ and naphth.), 4.35 (s, 6 H, methyl), 2.70 (s, 3 H, CH) ppm.

Supporting Information (see footnote on the first page of this article): FTIR spectra of the compounds are presented.

Acknowledgments

We are grateful to the Fundação para a Ciência e a Tecnologia (FCT), the Programa Operacional Ciência e Inovação (POCI) 2010, Orçamento do Estado (OE) and Fundo Europeu de Desenvolvimento Regional (FEDER) for funding (Project POCI/CTM/58507/2004). S. M. B. thanks the FCT for a doctoral grant.

[1] a) C. T. Kresge, M. E. Leonowicz, W. J. Roth, J. C. Vartuli, J. S. Beck, *Nature* **1992**, *359*, 710–712; b) J. S. Beck, J. C. Vartuli, W. J. Roth, M. E. Leonowicz, C. T. Kresge, K. D. Schmitt, C. T. W. Chu, D. H. Olson, E. W. Sheppard, S. B. McCullen,

J. B. Higgins, J. L. Schlenker, *J. Am. Chem. Soc.* **1992**, *114*, 10834–10843.
[2] a) J. Y. Ying, C. P. Mehnert, M. S. Wong, *Angew. Chem. Int. Ed.* **1999**, *38*, 56–77; b) K. Ariga, A. Vinu, J. P. Hill, T. Mori, *Coord. Chem. Rev.* **2007**, *251*, 2562–2591.
[3] a) K. Moller, T. Bein, *Chem. Mater.* **1998**, *10*, 2950–2963; b) A. Vinu, K. Z. Hossain, K. Ariga, *J. Nanosci. Nanotechnol.* **2005**, *5*, 347–375.
[4] a) I. J. Shannon, T. Maschmeyer, R. D. Oldroyd, G. Sankar, J. M. Thomas, H. Pernot, J. P. Balikdjian, M. Che, *J. Chem. Soc. Faraday Trans.* **1998**, *94*, 1495–1499; b) P. Ferreira, I. S. Gonçalves, F. E. Kühn, M. Pillinger, J. Rocha, A. M. Santos, A. Thursfield, *Eur. J. Inorg. Chem.* **2000**, 551–557; c) S. O'Brien, J. M. Keates, S. Barlow, M. J. Drewitt, B. R. Payne, D. O'Hare, *Chem. Mater.* **1998**, *10*, 4088–4099; d) P. Ferreira, I. S. Gonçalves, F. Mosselmans, M. Pillinger, J. Rocha, A. Thursfield, *Eur. J. Inorg. Chem.* **2000**, 97–102; e) J. M. Campos, M. R. Ribeiro, J. P. Lourenço, A. Fernandes, *J. Mol. Catal. A* **2007**, *277*, 93–101.
[5] a) C. D. Nunes, A. A. Valente, M. Pillinger, J. Rocha, I. S. Gonçalves, *Chem. Eur. J.* **2003**, *9*, 4380–4390; b) S. M. Bruno, B. Monteiro, M. S. Balula, F. M. Pedro, M. Abrantes, A. A. Valente, M. Pillinger, P. Ribeiro-Claro, F. E. Kühn, I. S. Gonçalves, *J. Mol. Catal. A* **2006**, *260*, 11–18.
[6] a) A. N. Gleizes, A. Fernandes, J. Dexpert-Ghys, *J. Alloys Compd.* **2004**, *374*, 303–306; b) A. Fernandes, J. Dexpert-Ghys, A. Gleizes, A. Galarneau, D. Brunel, *Microporous Mesoporous Mater.* **2005**, *83*, 35–46.
[7] a) S. Gago, J. A. Fernandes, J. P. Rainho, R. A. Sá Ferreira, M. Pillinger, A. A. Valente, T. M. Santos, L. D. Carlos, P. J. A. Ribeiro-Claro, I. S. Gonçalves, *Chem. Mater.* **2005**, *17*, 5077–5084; b) C. Peng, H. Zhang, J. Yu, Q. Meng, L. Fu, H. Li, L. Sun, X. Guo, *J. Phys. Chem. B* **2005**, *109*, 15278–15287; c) L. N. Sun, H. J. Zhang, C. Y. Peng, J. B. Yu, Q. G. Meng, L. S. Fu, F. Y. Liu, X. M. Guo, *J. Phys. Chem. B* **2006**, *110*, 7249–7258; d) L. N. Sun, J. B. Yu, H. J. Zhang, Q. G. Meng, E. Ma, C. Y. Peng, K. Y. Yang, *Microporous Mesoporous Mater.* **2007**, *98*, 156–165.
[8] P. Escribano, B. Julián-López, J. Planelles-Aragó, E. Cordoncillo, B. Viana, C. Sanchez, *J. Mater. Chem.* **2008**, *18*, 23–40.
[9] a) G. F. de Sá, O. L. Malta, C. D. Donegá, A. M. Simas, R. L. Longo, P. A. Santa-Cruz, E. F. da Silva, *Coord. Chem. Rev.* **2000**, *196*, 165–195; b) K. Binnemans in *Handbook on the Physics and Chemistry of Rare Earths* (Eds.: K. A. Gschneidner Jr, J.-C. G. Bünzli, V. K. Pecharsky), Vol. 35, Elsevier, Amsterdam, **2005**, ch. 225, pp. 107–272.
[10] a) J. A. Fernandes, R. A. Sá Ferreira, M. Pillinger, L. D. Carlos, J. Jepsen, A. Hazell, P. Ribeiro-Claro, I. S. Gonçalves, *J. Lumin.* **2005**, *113*, 50–63; b) A. Bellusci, G. Barberio, A. Crispini, M. Ghedini, M. La Deda, D. Pucci, *Inorg. Chem.* **2005**, *44*, 1818–1825; c) J. A. Fernandes, R. A. Sá Ferreira, M. Pillinger, L. D. Carlos, I. S. Gonçalves, P. J. A. Ribeiro-Claro, *Eur. J. Inorg. Chem.* **2004**, 3913–3919; d) D. F. Moser, L. C. Thompson, V. G. Young Jr, *J. Alloys Compd.* **2000**, *303–304*, 121–124; e) V. Tsaryuk, J. Legendziewicz, L. Puntus, V. Zolin, J. Sokolnicki, *J. Alloys Compd.* **2000**, *300–301*, 464–470.
[11] a) C. Benelli, A. Caneschi, A. C. Fabretti, D. Gatteschi, L. Pardi, *Inorg. Chem.* **1990**, *29*, 4153–4155; b) C. Pettinari, F. Marchetti, R. Pettinari, A. Drozdov, S. Troyanov, A. I. Voloshin, N. M. Shavaleev, *J. Chem. Soc., Dalton Trans.* **2002**, 1409–1415; c) M. Shi, F. Li, T. Yi, D. Zhang, H. Hu, C. Huang, *Inorg. Chem.* **2005**, *44*, 8929–8936; d) P. P. Lima, R. A. Sá Ferreira, R. O. Freire, F. A. Almeida Paz, L. S. Fu, S. Alves, L. D. Carlos, O. L. Malta, *ChemPhysChem* **2006**, *7*, 735–746.
[12] A. Abbasi, E. D. Risberg, L. Eriksson, J. Mink, I. Persson, M. Sandström, Y. V. Sidorov, M. Y. Skripkin, A. S. Ullström, *Inorg. Chem.* **2007**, *46*, 7731–7741.
[13] a) B. Marler, U. Oberhagemann, S. Vortmann, H. Gies, *Microporous Mater.* **1996**, *6*, 375–383; b) W. Hammond, E. Prouzet, S. D. Mahanti, T. J. Pinnavaia, *Microporous Mesoporous Mater.* **1999**, *27*, 19–25.
[14] S. J. Gregg, K. S. W. Sing in *Adsorption, Surface Area and Porosity*, 2nd ed., Academic Press, London, **1982**.
[15] a) M. D. Alba, A. I. Becerro, J. Klinowski, *J. Chem. Soc. Faraday Trans.* **1996**, *92*, 849–854; b) A. A. Romero, M. D. Alba, W. Zhou, J. Klinowski, *J. Phys. Chem. B* **1997**, *101*, 5294–5300.
[16] Y. H. Zhao, M. H. Abraham, A. M. Zissimos, *J. Org. Chem.* **2003**, *68*, 7368–7373.
[17] L. Fu, R. A. Sá Ferreira, A. Valente, J. Rocha, L. D. Carlos, *Microporous Mesoporous Mater.* **2006**, *94*, 185–192, and references therein.
[18] K. Ray, A. Shanzer, D. H. Waldeck, R. Naaman, *Phys. Rev. B* **1999**, *60*, 13347–13350.
[19] a) S. T. Frey, W. D. Horrocks Jr., *Inorg. Chim. Acta* **1995**, *229*, 383–390; b) O. L. Malta, H. J. Batista, L. D. Carlos, *Chem. Phys.* **2002**, *282*, 21–30; c) L. D. Carlos, O. L. Malta, R. Q. Albuquerque, *Chem. Phys. Lett.* **2005**, *415*, 238–242; d) L. D. Carlos, A. L. L. Videira, *J. Chem. Phys.* **1994**, *101*, 8827–8830; e) C. K. Jørgensen, *Prog. Inorg. Chem.* **1962**, *4*, 73–124.
[20] R. G. Charles, A. Perrotto, *J. Inorg. Nucl. Chem.* **1964**, *26*, 373–376.
[21] C. D. Nunes, A. A. Valente, M. Pillinger, A. C. Fernandes, C. C. Romão, J. Rocha, I. S. Gonçalves, *J. Mater. Chem.* **2002**, *12*, 1735–1742.

Received: April 10, 2008
Published Online: July 10, 2008

